Extension of Automotive Radar Target List Simulation to consider further Physical Aspects

Markus Bühren and Bin Yang
Chair of System Theory and Signal Processing
University of Stuttgart, Germany
www.LSS.uni-stuttgart.de

***Abstract*— In many areas of signal processing, developers use simulated data in the design of new algorithms. One advantage of simulated data is that it gives an exact reference and thus allows to compute objective error measures. In the field of automotive radar, however, real data is often used from the beginning because of the high complexity of the underlying electromagnetic wave model. In [1, 2], we have presented a model for the simulation of automotive radar target lists – i.e. the measured distance, bearing angle, Doppler velocity and amplitude of detected targets – that is very attractive in terms of implementational and computational effort, compared to, for example, a finite-element or ray-tracing model. The simulation serves as a tool for the development of radar signal processing algorithms which start with the radar target list as input data, for example algorithms for tracking or data fusion. In this paper, we will present extensions to the existing model which consider the effects of multipath propagation and multiple reflections in order to bring the simulated target lists a step closer to reality.**

***Index Terms*— Radar simulation, Radar signal processing, Road vehicle radar**

I. Review of simulation model

The simulation model can roughly be split into two parts. The first part is a model of the objects under consideration, in our case mainly vehicles. The representation of objects is not specific for the radar sensor we are modeling (a Tyco Electronics M/A-Com 24 GHz short range radar sensor [3]), but can be used for other radar sensors with similar resolution capabilities as well. As shown in Fig. 1, a vehicle is represented by a small number of *point reflection centers* (the angular sectors A-H represent their visibility regions) and circular *plane reflectors* (thick lines with end points marked). The radar cross sections of the given reflectors can be derived by comparison of simulated data with measurement data.

Given a traffic situation (i.e. positions and velocities of vehicles) and the object representation, an ideal target list can be computed simply by geographical considerations. The task of the second part of the simulation model, the sensor model, is to transform this ideal target list into a realistic one, with the detection, resolution and noise characteristics of the real counterpart considered.

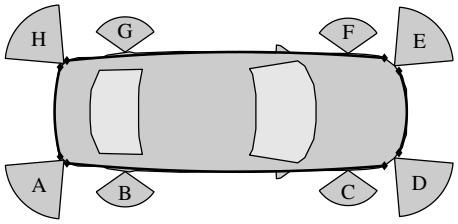

Fig. 1. Vehicle reflection model

In the sensor model, first the measured amplitude is computed by considering distance, antenna pattern and object RCS. If this amplitude exceeds a certain threshold, a target is said to be detected. After that, the limited resolution capabilities are simulated by distributing the targets on resolution cells. For each resolution cell containing a detected target, the angle estimation procedure of the real sensor is imitated and artificial noise is added to the measurements of distance and Doppler speed. Finally, the sensor-internal tracking, which serves to filter clutter and smooth the noisy estimations, is simulated.

The model as described until now ignores certain physical effects. We will explain how we simulate the interference pattern caused by multipath propagation in section II. In section III an approach is presented how to incorporate multiple ping-pong reflections between observer and object into the simulation model.

II. Multipath propagation

In our model, the amplitude of a radar target (in dB) was coarsely approximated as a linear function of the distance to the target so far. This simple model was derived from real radar measurements, but significant decays in the amplitude at certain distances were

ignored. These decays are caused by multipath propagation. The main part of the emitted radar energy will travel on the direct path from the sensor to the object and take the same path back to the sensor. But as the road surface, which works as a planar reflector, is always present in automotive radar applications, a part of the radar energy will travel on indirect paths, i.e. *sensor – object – road surface – sensor* or, similarly, *sensor – road surface – object – sensor*. Also two ground reflections are possible, i.e. *sensor – road surface – object – road surface – sensor*.

The different paths have different lengths, and thus the reflected radar energy arrives at the receiving antenna with different delays. The superposition of several delayed versions of the emitted signal waveform leads to interference effects which are responsible for the decays in the received amplitude. The destructive interference can be so severe that corner reflectors or even vehicles are not detected at certain distances. Clearly, it is essential to include this physical effect in a target list simulation.

In Fig. 2, a set of real radar amplitude measurements is shown. In the measurement experiment, the observing vehicle was slowly approaching a corner reflector. The dots mark the measured amplitude at the measured distances. The amplitude is quantized with a quantization step size of 2 dB; closely spaced samples thus form horizontal lines. The lowest measured amplitude value was 0 dB, the largest 28 dB (clipped). At certain distances (for example at around 6.5 m, 8 m, 9.5 m and 12.5 m) sharp decays of the amplitude are visible. Between 16.5 and 20.5 m, no measurements are visible, which means that the decay is so deep that the corner reflector was not detected at all in that region.

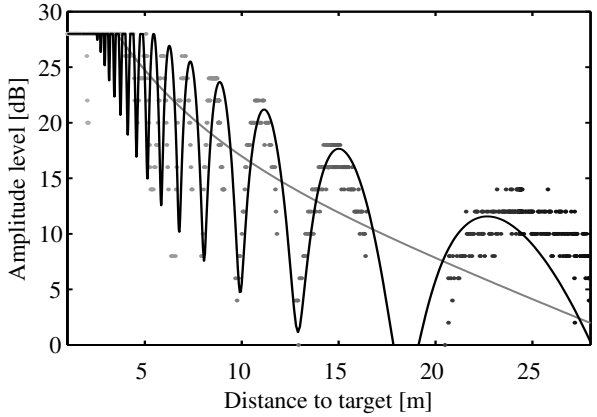

Fig. 2. Measured (dots) and simulated (line) radar amplitude of corner reflector measurement

The simulated amplitude (before quantization) is shown by the black line. It consists of a direct-path part (shown in gray) plus an interference part.

A. Direct-path amplitude

First we will describe a model for the direct-path amplitude (in dB) depending on the distance to the target. This model is not a low-level physical model, but was derived by inspection of real measurement data. The relation between the received signal power P_r, the transmitted signal power P_t and the distance R to the target is described by the well-known radar equation

$$P_r = \frac{P_t\, G_t\, A_r\, \sigma_{\text{target}}}{(4\pi)^2 R^4}. \qquad (1)$$

Here, G_t is the transmit antenna gain and A_r is the receiving antenna aperture area. In many radar applications, the radar cross section (RCS) σ_{target} and the transmit antenna gain G_t can be approximated as constant, for example when observing an aircraft many kilometers away. In that case, the famous "$1/R^4$-law" of the signal power depending on the target range holds true. However, in automotive radar applications, the target distances are comparably small. A vehicle in a distance of two meters, for example, clearly is not completely illuminated by the radar. The radar cross section σ_{target} can thus not be seen as constant and the $1/R^4$-law is not applicable in that simple isolated way.

A second fact prohibits to build a physical amplitude simulation. In common automotive radar receivers (for example as described in [4]), a sensitivity time control (STC) (also called gain time control, GTC) is used. In order to enhance the dynamic range of the receiver, the signal amplification is chosen lower for closer targets and higher for targets further away. As we do not have any information from the sensor manufacturer about the applied gain control in the sensor we are modeling, we are not able to build a detailed physical model for the received amplitude.

As stated before, a linear function of the amplitude in dB over the distance to the target was formerly used as an approximation for the direct-path amplitude. However, at small distances, the resulting simulated amplitude values were far too small. The clearly visible clipping of the amplitudes at 28 dB was not well represented. Selecting a higher (negative) slope resulted in unrealistically large values at intermediate distances. The linear model was thus improved by adding an exponential term, which results in the following function:

$$L(A_{\text{dp}}(R)) = k_1 + k_2\, R + k_3\, \mathrm{e}^{k_4 R} + L(\text{ERCS}) \quad (2)$$

Here we used the level operator L with $L(x) = 20\log(x/x_0)$ dB which transforms the given values

from a linear to a logarithmic scale. The terms $k_1 + k_2\,R$ forms a linear function, while the following term, $k_3 \exp(k_4 R)$, represents the exponentially decreasing correction of the simple linear model. The following parameters were found by comparison with real measurement data:

k_1	k_2	k_3	k_4
20.5 dB	-0.7 dB/m	19.5 dB	-0.2 m^{-1}

The abbreviation ERCS in equation (2) stands for "Equivalent RCS". As we do not have any information about the relation between the amplitude value in dB read from the sensor to the received power at the radar front end, we can not give the RCS of objects in m^2. Hence, we use a proportional measure here. The value ERCS $= 1$ or $L(\mathrm{ERCS}) = 0$ dB was arbitrarily assigned to the corner reflector used in this measurement. Other objects like vehicles or trucks will be assigned equal or larger values, pedestrians typically smaller values.

B. Interference pattern

The interference pattern of the amplitude over the distance, which is clearly visible in Fig. 2 as sharp decays in the measured amplitudes, is caused by multipath propagation. The situation is schematically shown in Fig. 3. Here, the sensor is positioned in height h_1 on the z-axis. The object, at this moment viewed as a point target, is at a distance R from the radar sensor in height h_2. In automotive applications, the mounting height of radar sensor on a car will be around 30-60 cm, on a truck possibly slightly higher. The height of the main reflection points on object vehicles can be expected to be in the range of 30 cm to 1 m for common vehicle models. The following factors influence the interference pattern:

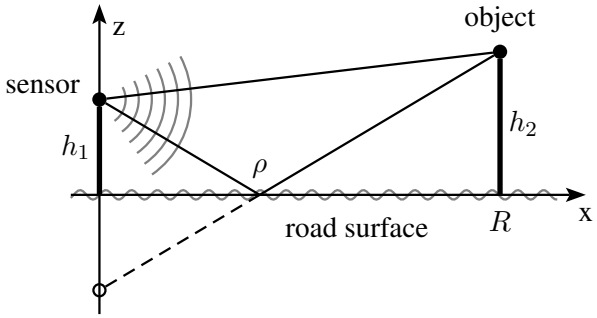

Fig. 3. Path length difference at ground reflection

1) The phase difference caused by different path length.
2) The phase shift and attenuation caused by the reflection at the road surface.
3) The path attenuation (amplitude decreasing with $1/R^4$ according to the radar equation).
4) The antenna elevation pattern.
5) The reflector elevation pattern.

The first two factors are the most important ones and will be discussed in detail. The influence factors 3) and 4) are expected to cause significant differences only for small target distances, but will also be taken into account here as they are simple to formulate. Finally, the reflector elevation pattern, i.e. a different reflectivity or radar cross section depending on the impinging angle, is not considered here, as effects of such fine granularity can not be reasonably modeled by a simple comparison with real measurement data.

In order to compute the phase difference and amplitude attenuation caused by the different path length, we first compute the length of the paths. The direct path from sensor to object has the length

$$d_{\mathrm{dp}}(R) = \sqrt{(h_2 - h_1)^2 + R^2}, \tag{3}$$

while the length of the propagation path *sensor – road surface – object* is

$$d_{\mathrm{rp}}(R) = \sqrt{(h_2 + h_1)^2 + R^2}. \tag{4}$$

Thus, the complete path lengths – from sensor to object and back – are $d_0(R) = 2d_{\mathrm{dp}}(R)$ for the direct reflection, $d_1(R) = d_{\mathrm{dp}}(R) + d_{\mathrm{rp}}(R)$ for the two different paths with one ground reflection, and $d_2(R) = 2d_{\mathrm{rp}}(R)$ for the path that includes two ground reflections. The corresponding travel way differences are

$$\Delta d_1(R) = d_{\mathrm{rp}}(R) - d_{\mathrm{dp}}(R) \quad \text{and} \tag{5}$$

$$\Delta d_2(R) = 2(d_{\mathrm{rp}}(R) - d_{\mathrm{dp}}(R)). \tag{6}$$

The phase differences to the direct path result in

$$\Delta\varphi_1(R) = 2\pi\frac{\Delta d_1(R)}{\lambda} = 2\pi\frac{d_{\mathrm{rp}}(R) - d_{\mathrm{dp}}(R)}{\lambda} \tag{7}$$

and

$$\Delta\varphi_2(R) = 2\pi\frac{\Delta d_2(R)}{\lambda} = 4\pi\frac{d_{\mathrm{rp}}(R) - d_{\mathrm{dp}}(R)}{\lambda}. \tag{8}$$

With this, the interference pattern $p(R)$ has the form

$$p(R) = 1 + a_1(R)\,\mathrm{e}^{\Delta\varphi_1(R)} + a_2(R)\,\mathrm{e}^{\Delta\varphi_2(R)}, \tag{9}$$

where the complex factors $a_1(R)$ and $a_2(R)$ are derived in the following. Note that all contributions are normalized to the direct path.

The radar energy that travels once or twice the reflection path is attenuated differently from the direct

path. The first effect to cause the attenuation is the path loss due to the longer way of travel. According to the radar equation (1), the attenuation is proportional to $1/R^4$. Before it was stated that the $1/R^4$-law can not be observed in automotive radar data. However, of course the radar equation still holds, it is just that other terms except the target distance R are changing as well. The attenuation due to the different way of travel, normalized to the direct path, is thus

$$a_{1/2}^{\mathrm{pl}}(R) = \left(\frac{d_0(R)}{d_{1/2}(R)} \right)^4 \tag{10}$$

with $d_0(R)$, $d_1(R)$ and $d_2(R)$ as defined in the text above equation (5).

Another important effect to be considered is the reflection on the road surface itself. The reflection can introduce an attenuation as well as a phase shift. Regarding to the literature about radar wave propagation [5], the complex ground reflection coefficient ρ with $|\rho| < 1$ depends on the surface, the wavelength and the angles of incidence and reflection. On a perfectly smooth surface with angles close to zero (i.e. for large distances between sensor and target), the ground reflection coefficient is $\rho = -1$, i.e. no attenuation but a phase shift of π.

However, in our case we neither have a perfectly smooth surface nor are the angles of incidence and reflection very small. Even if the ground reflection coefficient depends on the mentioned two angles and thus on the distance R, we use a constant complex parameter ρ here. Increasing its magnitude leads to higher maxima and lower minima in the interference pattern, while a change of the phase will shift the maxima and minima to higher or lower distances R. By comparison with different real measurement sets, the value $\rho = 0.5\,\mathrm{e}^{j\frac{\pi}{3}}$ turned out to be a good compromise. The phase of this value is far away from the before mentioned phase of a perfectly smooth surface. But with a phase of π, the resulting interference patterns are totally wrong. Considering that the ground reflection will influence the radar amplitude and phase at each reflection, we get the contributions

$$a_1^{\rho}(R) = \rho \quad \text{and} \quad a_2^{\rho}(R) = \rho^2 \tag{11}$$

The last influence on the factors $a_1(R)$ and $a_2(R)$ is given by the transmit- and receive elevation pattern. We have included this in our simulation even if the influence is very small. At larger distances, the impinging angles of the direct and reflected rays do not differ very much, and so the corresponding elevation patterns will be very similar. At smaller distances, the influence of the elevation pattern is larger, but for many objects the amplitude will be in the clipping region anyway. Due to this, we omit the discussion of the antenna model here and do not define the parameters $a_1^{\mathrm{el}}(R)$ and $a_2^{\mathrm{el}}(R) = (a_1^{\mathrm{el}}(R))^2$ here. They can be set to 1 without introducing large differences.

Summarizing, the interference pattern $p(R)$ of equation (9) can be computed with the factors

$$a_{1/2}(R) = a_{1/2}^{\mathrm{pl}}(R) \cdot a_{1/2}^{\rho}(R) \cdot a_{1/2}^{\mathrm{el}}(R). \tag{12}$$

The resulting pattern is shown in Fig. 2 as a black line.

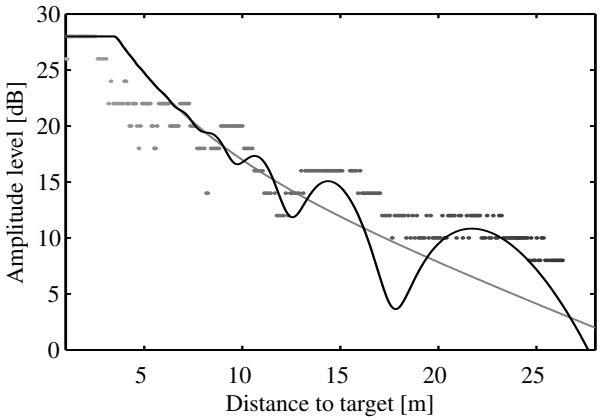

Fig. 4. Measured (dots) and simulated (line) radar amplitude of measurement with Opel Vectra as target

The agreement between the simulated radar data and the real measurement data of the corner reflector experiment is fairly good – at least when viewing the simulation as a tool for the development of tracking algorithms, as it was designed for. However, this is not the case for extended objects like a car. In Fig. 4 the amplitude measured when approaching the front of an Opel Vectra is shown. Clearly, the interference pattern is significantly different from that of the corner reflector in Fig. 2.

In contrast to the corner reflector, which approximately acts as a point target, a vehicle is an extended object. In order to take this fact into account in the simulation, we changed our representation of reflection centers. Instead of a representation as a single point reflector like in Fig. 3, we use a number of point reflectors in different heights as shown in Fig. 5. The path length differences between all direct and reflected paths are different and lead to different interference patterns. In the simulation, all these patterns are computed for the current value of R; the final overall interference pattern between the sensor and the extended object is then set as the average of all subpatterns. The averaging leads to a smoothing of the single-reflector interference pattern, as the positions of maxima and minima vary for different re-

flector heights. The averaging effect has the largest influence at small distances, where the minima and maxima are very close together.

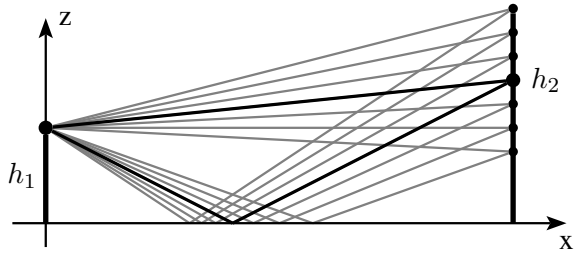

Fig. 5. Path length averaging principle

In order to attain the simulated amplitude of the Opel Vectra in Fig. 4, we used 11 subreflectors with a spacing of 1 cm in between. The resulting representation thus spans a height of 10 cm between the uppermost and the lowermost subreflectors. The center reflector was placed at a height of 50 cm. The agreement between simulated and real data is sufficient for our needs, but clearly leaves space for improvement.

Even for the simulation of the measurement data of the corner reflector experiment shown in Fig. 2, the averaging over different heights was used. Here, averaging over 5 interference subpatterns or 4 cm in height was applied. Without averaging, the simulated amplitude would look as shown in Fig. 6. The oscillations at small distances are unrealistically large without application of the averaging procedure.

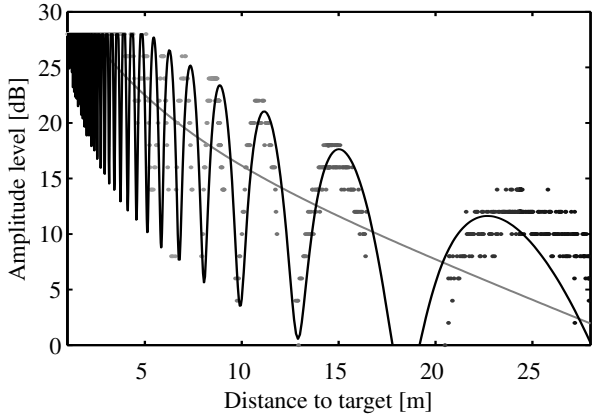

Fig. 6. Measured (dots) and simulated (line) radar amplitude of corner reflector without averaging

Note that interference patterns would be implicitly included in an electromagnetic wave propagation simulation on a lower level, e.g. in a ray-tracing simulation. However, the representation we are using is much simpler and requires orders of magnitudes less computation time.

III. Multiple reflections

If the distance between sensor and object gets small, the influence of multiple reflections becomes visible. As the sensor-equipped vehicle itself is a good reflector for electromagnetic waves, it will reflect the radar energy that was already reflected by objects once more. Parts of that energy will again be reflected at the object and find their way back to the receiving antenna of the radar sensor.

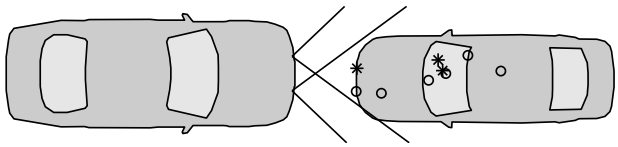

Fig. 7. Measured target lists with multiple reflections

If distances are small, the radar waves that take the path *sensor – object – observing vehicle – object – sensor* is often still strong enough to be detected. The travel path is twice as long as the direct path (*sensor – object – sensor*), thus ghost targets appear at around two times the true distance to the object due to ping-pong reflections between observing vehicle and object. We have observed this effect in measurements with realistic traffic scenarios up to an reflection order of three, i.e. at three times the distance to the original reflector. This is well observable in Fig. 7, where the target list of a single frame is shown in bird's eye view. The stars indicate the targets detected by the left sensor, while circles mark the detections of the right sensor. Besides the detections on the front of the object vehicle, at roughly two times the distance from the sensor, i.e. on the object's windshield, a lot of ghost targets are visible. On the vehicle's roof, a single detection at around three times the distance is visible. The front detections and the ghost targets can be seen as roughly lying on one line. This supports the assumption that the ghost targets stem from ping-pong reflections.

In our simulation, an object vehicle is represented by point reflection centers and plane reflectors. Depending on the current positions of observer and object, for each plane reflector a single reflection point is computed, so that finally only distinct points are left. For each of these points, the received amplitude is computed as described in the last section. If a target is said to be detected, the distance, angle and relative speed are computed [1,2]. In order to incorporate ghost targets caused by multiple reflections into the simulation, for each reflection center we generate additional targets under certain conditions. If the original reflector is less than 4 m away, ghost target candidates up to an reflection order of 3 (i.e. up to three times the distance to the original target) are generated. The limitations in distance and reflection order reduce

the computation effort of the simulation.

In order to cause a ghost target at about q times the original distance, the radar energy has to travel q times that distance. Path loss and sensitivity/gain time control depending on the traveled distance apply in the same way as the original reflection. The direct-path amplitude of a ghost target candidate is thus simulated according to equation (2) with the distance qR.

The interference occurring on the path traveled q times can, in contrast, not be computed as in equation (9), because the geometry is different. Here, the possible paths over the road surface are traveled q times and thus the computed interference pattern has to be applied q times, i.e. using $p^q(R)$ with the original distance R.

On a multiple reflection path there are $2q$ reflections involved, namely q reflections at the object and q reflections at the front of the observer. At each reflection, large parts of the impinging energy are lost. The exact relationship between the geometries of the involved vehicles are very complicated and only to be solved numerically by wave propagation simulations. In our simulation, however, we approximate the loss due to the additional reflections by a constant reflection loss of -13 dB per additional way. This parameter value, as most other parameter values, was found by visually comparing the results of the simulation with real measurement data.

After considering the direct-path amplitude, the interference pattern and the reflection loss, the amplitude for each ghost target candidate is available. If this is larger than 0 dB (the lowest amplitude the sensor returns), a ghost target is said to be detected and will be represented by an additional entry in the final target list. Now, the true values of distance, bearing angle and relative speed of the ghost targets that an ideal sensor (i.e. a sensor with unlimited accuracy and resolution and no noise) would measure, have to be computed. We expect that the ghost targets will be lying approximately on a line. For this, we use the original bearing angle, q times the original distance and q times the original relative speed. In order to simulate deviations from the ideal line constellation, we add noise of the following standard deviations to the ideal values:

σ_R	σ_{bearing}	$\sigma_{\text{rel. speed}}$
1 m	6°	0.2 m/s

The measurement noise is later added to these true values and the simulated sensor-internal tracking will then smooth the noisy target measurements (see [1, 2]). Because of the data association step in the internal tracking, ghost targets will only appear in the final target list if several detections accumulate at the same position. This matches well with the operation in a real sensor. The result is – for our needs – sufficiently close to reality, as Fig. 8 shows. Here the simulated counterpart of the same situation as in Fig. 7 is shown. Without further knowledge, it would not be possible to decide which of the target lists in Figs. 7 and 8 is the real measurement data.

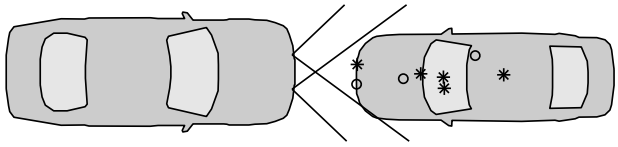

Fig. 8. Simulated target lists with multiple reflections

IV. Conclusion

In this paper we have presented two extensions to an existing radar target list simulation. The first one significantly improves the simulated amplitude by taking interference effects caused by multipath propagation into account. The simulated interference patterns show good compliance with a real measurement with a corner reflector as a target. The results with an extended object as targets are sufficiently accurate for our needs, but may still be improved.

Further we have shown how ghost targets that occur due to ping-pong reflection between observing vehicle and object vehicle at small distances can realistically be simulated. Additional reflectors are dynamically added and then treated as the original reflectors of the object model. The resulting simulated target lists are hard to distinguish from their real counterparts, which shows the feasibility of our approach.

References

[1] Markus Bühren and Bin Yang, "Simulation of automotive radar target lists using a novel approach of object representation," in *Proc. IEEE Intelligent Vehicles Symposium*, Tokyo, Japan, June 2006, pp. 314–319.

[2] Markus Bühren and Bin Yang, "Automotive radar target list simulation based on reflection center representation of objects," in *Proc. Intern. Workshop on Intelligent Transportation (WIT)*, Hamburg, Germany, Mar. 2006, pp. 161–166.

[3] Hermann Henftling, Dirk Klotzbücher, and Christian Frank, "Ultra wide band 24GHz sequential lobing radar for automotive applications," in *Proc. Intern. Radar Symposium (IRS)*, Berlin, Germany, Sept. 2005, pp. 79–82.

[4] Markus Wintermantel, "High efficient signal processing in a radar based ACC-system," in *Proc. Intern. Radar Symposium (IRS)*, Dresden, Germany, Sept. 2003, pp. 131–136.

[5] Merrill Skolnik, *Radar Handbook*, McGraw-Hill, 2nd edition, 1990.